Evaluation of rheology and strength development of alkali-activated slag with different silicates sources

Sun, Yubo; Ghorbani, Saeid; Dai, Xiaodi; Ye, Guang; De Schutter, Geert

Important note
To cite this publication, please use the final published version (if applicable).
Please check the document version above.

Evaluation of rheology and strength development of alkali-activated slag with different silicates sources

Yubo Sun [a], Saeid Ghorbani [a], Xiaodi Dai [a], Guang Ye [a,b], Geert De Schutter [a,*]

[a] *Magnel-Vandepitte Laboratory, Department of Structural Engineering and Building Materials, Ghent University, 9052, Ghent, Belgium*
[b] *Microlab, Section of Materials and Environment, Faculty of Civil Engineering and Geosciences, Delft University of Technology, Stevinweg 1, 2628 CN, Delft, the Netherlands*

ABSTRACT

This study provides a detailed investigation on the reproducibility of two groups of alkali-activated slag (AAS) mixtures, from both fresh properties and strength development perspectives. Three different commercial sodium silicate solutions and one lab-produced silicate activator (made of silica fume and sodium hydroxide) were used to prepare AAS pastes with the same nominal composition in each group. The reaction process of each AAS mixture was monitored by calorimetry and ultrasonic pulse velocity (UPV) measurements. Meanwhile, mini-slump and flow curve tests measured by rheometer were conducted in the first hour to characterize the evolution of fresh properties. The compressive and flexural strength of hardened AAS mortars were measured at different curing ages. The results revealed that AAS pastes prepared with three different sodium silicate solutions exhibited almost identical reaction kinetics, as well as the evolution of fresh properties and strength development. However, the reaction took place rather fast in AAS pastes made of silica fume. These mixtures showed worse rheology and less strength than the corresponding mixtures prepared with sodium silicate solutions. Furthermore, the present study also showed the feasibility of making the same AAS paste through different class commercial sodium silicate solutions.

1. Introduction

Alkali-activated materials (AAMs) are considered as a promising green alternative binder to replace ordinary Portland cement (OPC) in concrete constructions [1–4]. Their carbon footprint can be low [5,6] (depending, however, on the type of activator), and the mechanical [2, 7] and long-term properties [8–11] of AAM are equivalent or even better compared to OPC materials. Despite these advantages, the application of AAM is limited by the local availability of raw materials [3,12], and a generally accepted standard to classify and reduce variability of the properties of raw materials is still absent [13]. AAM is produced from industrial by-products (i.e. precursor) together with the activator [1,5], which provides high alkalinity to promote the dissolution of precursors. Among all of the alkaline substances, sodium hydroxide and sodium silicate are the most frequently used ones in reported studies, considering both industrial relevance and the properties of AAM [1,14,15].

Unlike sodium hydroxide, which has a fixed chemical composition. Sodium silicate is a generic appellation, involving a series of alkaline silicate substances in the form of $Na_{2x}SiO_{2+x}$ [16]. As a low-cost silica

source, sodium silicate is widely used in various industrial applications, such as sealants, deflocculates, emulsifiers, detergents, and adhesives [17,18]. The properties of commercial sodium silicate solutions are usually characterized by two factors, namely the SiO_2 content and the modulus (Ms) defined as the molar ratio between SiO_2 and Na_2O [18, 19]. Yang et al. [17] reported that the viscosity of sodium silicate solution increases with solid concentration raising from 15% to 55%, and reaches a minimum value at modulus of 1.8. Dimas et al. [20] determined that the hydrolytic stability and hardness of sodium silicate gel are proportional to the modulus. A few studies also reported silicate speciation variation by ^{29}Si NMR spectra [21–23] in sodium silicate, showing that more monomers and dimers were predominant in low modulus solutions, while larger oligomers and polymeric species were detected as the modulus increased.

In addition to the inherent properties of sodium silicate solutions, the composition of the activator (i.e. the synthesized sodium silicate solution) is further modified by the sodium hydroxide and water content involved. The silicate speciation, structures and interactions in sodium silicate solutions under external perturbations have been intensively

---

investigated in chemical engineering studies. McGarry et al. [24] found out that silicate anions polymerized into higher polymeric species or colloids as the concentration of hydroxyl ions and pH reduced during the dilution process. Bass et al. [25] also stressed that the extent of polymerization of silicate species depends on both alkalinity and degree of dilution. Nordström et al. [18] schematically illustrated the gelation process of sodium silicate solution. They proposed that the silicate speciation remains unchanged by increasing the concentration while lowering pH leads to condensation between low molecular weight species. Dietzel and Usdowski [26] studied the aging effect of diluted sodium silicate solution, and concluded that the polymerization rate of silicate species is governed by the alkalinity, SiO_2, and electrolytes concentrations. Böschel et al. [19] further classified the silicate colloid size by dynamic light scattering study, and they also reported the silicate particle size variation due to the dilution process and aging effect. Given the different starting points from various grades of commercial sodium silicate solutions, as well as externally supplemented sodium hydroxide and water, there should be a certain dynamic exchanging process among silicate species in the activator until chemical equilibrium between monomeric and polymeric silicate anions [27] occurs. In that case, the property of activator is governed not only by the original sodium silicate and hydroxide fed into the solution but also the polysilicate equilibrium [21] processes in the activator.

The effects of different silicate species in the activator have been reported as well in a few AAM studies. Shi et al. [28] suggested that the adjusted silicate solution by adding sodium hydroxide may have different species as compared with the one manufactured directly. Weng and Crentsil [29] prepared activators out of silicates with various modulus to reach a fixed target composition, and significant distinctions have been observed in the heat evolution. They concluded that the alkalinity of activator is predominantly determined by the sodium hydroxide added, and will further influence especially the early-stage dissolution process, as well as the incorporation between Al ions dissolved from precursors and silicate species. Duxson et al. [22] predicted that the aluminate dissolved in high modulus activator would be incorporated in stable aluminosilicate species, while activator with low modulus will result in a large amount of labile aluminate and silicate monomer/dimer, and thus the gel structure is more labile than those synthesized in high modulus activators. Several studies have also confirmed that the setting behavior of AAM is sensitive to the modulus of activator [30–33], a reversion in initial setting time has been detected as modulus increases. Criado et al. [34] conducted NMR analyses on both prime materials and hardened pastes, and the results indicate that the polymerization degree of the predominant silica species in the activator has a great impact on the structure and composition of the gel initially formed. In general, previous studies revealed that different silicate speciation in the activator would bring a certain impact on the early-stage dissolution and polymerization process.

In the majority of published studies, it is generally accepted that the activator should be prepared one day before mixing by dissolving alkaline compounds into water and should cool down till room temperature. However, it is not clear how the modulus modification and polysilicate equilibrium processes will affect the silicate speciation in the activator, and whether they will have a further impact on the subsequent 'geopolymerization' process. Moreover, due to the limitation of locally available precursors and chemical products, a commonly applied AAM standard is not yet available, and the reproducibility of a good AAM mixture with local materials is still uncertain. Accordingly, essential questions arise as to whether the properties of activators made of sodium hydroxide and different silicates are identical, and is it possible to produce "the same" AAM with different silicates?

Therefore, the present research aims to evaluate the performance of silicate from different suppliers with various modulus and water content in the activator, as well as their effect on the properties of AAM. In this study, activators with the same nominal composition were prepared with three types of commercial sodium silicate solutions (SS) and silica fume (SF). Extra water and sodium hydroxide were applied to keep chemical composition constant among activators in the same group. Experiments on the reaction kinetics and fresh properties were conducted on paste level. Ultrasonic pulse velocity (UPV) and isothermal calorimetry measurements were performed to monitor the reaction process, while the fresh properties of AAS pastes were characterized by mini-slump and flow curve tests. Eventually, compressive and flexural strengths were checked at different curing ages, and the one-day reaction product was investigated by Fourier transform infrared spectroscopy (FTIR). The results indicate that it is possible to reproduce AAS mixtures with identical fresh and hardened properties by using different commercial sodium silicate solutions through the preparation protocol proposed in this study.

2. Experimental method

2.1. Materials

The blast furnace slag (BFS) used in this study was provided by Ecocem Benelux B.V., with a density of 2890 kg/m³. The particle size distribution measured by laser diffraction is given in Fig. 1(a), and the d_{50} is 8.28 μm. The chemical composition of BFS determined by XRF and LOI is shown in Table 1. Morphology of BFS particles was visualized by scanning electron microscopy (SEM), and angular particles with irregular shapes have been observed as shown in Fig. 1(b).

Sodium hydroxide and sodium silicate are combined as the activator to prepare the AAS mixtures in this study. Reagent-grade sodium hydroxide anhydrous pearls (>99.0%) were provided by Brenntag N.V. The silicate species in the activator originated from silica fume powder (SF) and three types of commercial sodium silicate (SS). SF used to prepare alkaline solutions is dark grey powder mostly consisting of SiO_2 with a bulk density of approximately 275 kg/m³ (undensified). The chemical composition of solid SF is shown in Table 1. Details of SS solutions are listed in Table 2, SS1 and SS2 were provided by PQ Corporation, and SS3 was provided by Brenntag N.V.

2.2. Mixture proportions

Eight AAS pastes were designed with two different nominal compositions (Low silicate dosage: 4% Na_2O, Ms = 0.25; High silicate dosage: 4%Na_2O, Ms = 0.5) [35], and the water to binder ratio (w/b) was kept constant at 0.4 in each mixture. Details of mix design are given in Table 3.

The alkaline activators were prepared by dissolving the alkaline and silicate compounds in tap water 24 h before mixing. Electromagnetic stirring was conducted at 150 rpm to promote the dissolution of alkaline and silicate substances, especially of the solid SF particles. The alkalinity of activators was determined by Extech PH150 pH-meter at 20 ± 0.5 °C, and the results are presented in Table 3.

2.3. Testing program

2.3.1. Characterization on activator solutions

The viscosity of each activator solution was determined by Anton Paar MCR 102 rheometer fitted with a concentric cylinder at 20 ± 0.5 °C. For each measurement, 15 mL activator solution was filled into the cup and external shear was applied by the cylinder at a constant low speed of 5 rpm for 60 s, and the average responsive viscosity was recorded by the program. The mean value of three measurements was reported as the viscosity of each activator solution.

It has been observed that in the activators of S4Ms0.25 and S4Ms0.5 mixtures, the SF particles were incompletely dissolved after 24 h. In that case, the actual silicate modulus in the SF-based activator was lower than those indicated in Table 3. Therefore, the mass of undissolved SF in S4Ms0.25 and S4Ms0.5 activator solutions were measured according to the method described in Ref. [36]. The actual Ms was subsequently
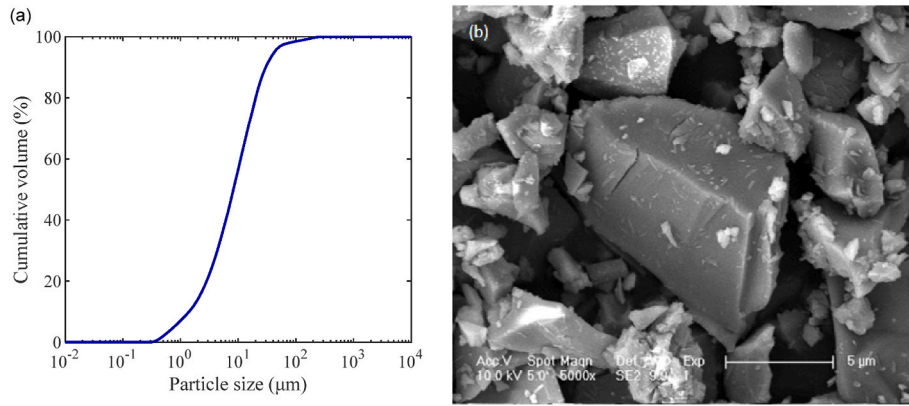
Fig. 1. Physical properties of BFS (a) Particle size distribution; (b) Morphology by SEM (5000 × magnification).

Table 1
Chemical composition of BFS measured by XRF and LOI (mass %).

Precursor	CaO	SiO$_2$	Al$_2$O$_3$	MgO	SO$_3$	TiO$_2$	K$_2$O	Fe$_2$O$_3$	MnO	ZrO$_2$	Other	LOI[a]
BFS	40.9	31.1	13.7	9.16	2.31	1.26	0.69	0.40	0.31	0.12	0.05	0.10
SF	0.3	97.0	0.7	0.4	0.1	–	0.8	0.1	–	–	0.6	–

[a] LOI measured by TG analysis at 950 °C.

Table 2
Chemical composition of sodium silicate solutions.

	Na$_2$O[a]	SiO$_2$[b]	Ms[c]	Water[d]
SS1	18	28.5	1.6	53.5
SS2	15	30	2.0	55
SS3	8	26.9	3.4	65.1

[a, b, d] Represented as mass percentage of sodium silicate solution.
[c] Defined as mass ratio between SiO$_2$ and Na$_2$O.

determined by Eq. (1) for further investigations.

$$Ms_{act} = \frac{(m_1 - \overline{m_2}) \times p(SiO_2)}{m(Na_2O)} \quad (1)$$

where:

Ms_{act} is the actual silicate modulus in SF-based activators.

m_1 is the mass of solid SF added into the alkaline solution in grams.

$\overline{m_2}$ is the mass of undissolved SF in grams (average value from 3 measurements).

$p(SiO_2)$ is the mass percentage of SiO$_2$ in SF (see Table 1).

$m(Na_2O)$ is the equivalent mass of Na$_2O$ in the activator.

2.3.2. Mixing protocol

The AAS pastes were blended with a Hobart mixer by mixing BFS with activators at low speed (140 rpm) and high speed (285 rpm) for 60 and 90 s, respectively. Fresh AAS pastes were used for further UPV, mini-slump, and rheology tests.

2.3.3. Isothermal calorimetry

The heat evolution of AAS pastes was monitored by the TAMAIR isothermal calorimeter. Fresh paste was prepared by manually mixing BFS and activator in a plastic cup for 2 min. Afterwards, 14 ± 0.01 g of AAS paste was immediately transferred into a glass ampoule. Subsequently, the ampoules were sealed and loaded into isothermal channels in the calorimeter, and the heat evolution along the reaction process was recorded at 20± 0.5 °C for 24 h. The heat flow and cumulative heat evolution present in this study were normalized into 1 g of solid binder (including precursors and solid activators).

2.3.4. Ultrasonic pulse velocity (UPV)

UPV in AAS paste was detected by FreshCon system [37] for 24 h after mixing, and the testing device was located in a chamber with 60% relative humidity and 20 ± 1 °C. In each test, the fresh AAS paste was

Table 3
Mixture proportion of AAS pastes.

Mix	BFS[a] (g)	Activator (g)							Na$_2$O[b]	SiO$_2$[c]	Ms[d]	w/b[e]
		Sodium hydroxide	Silicate				Water	pH				
			SS1	SS2	SS3	SF						
S1Ms0.25	400	17.39	14.04	0	0	0	162.05	13.65	4%	1%	0.25	0.4
S2Ms0.25		18.06	0	13.33	0	0	162.29	13.67				
S3Ms0.25		19.11	0	0	14.87	0	160.04	13.68				
S4Ms0.25		20.65	0	0	0	4	169.86	13.81				
S1Ms0.5		14.14	28.07	0	0	0	155.84	13.56		2%	0.5	
S2Ms0.5		15.48	0	26.67	0	0	156.33	13.57				
S3Ms0.5		17.58	0	0	29.74	0	151.82	13.54				
S4Ms0.5		20.65	0	0	0	8	171.46	13.68				

[a] The mass of precursor was fixed at 400 g for each mixture in this study.
[b, c] Represented as the total mass of Na$_2$O and SiO$_2$ in activator divided by the mass of precursor.
[d] Defined as the mass ratio between SiO$_2$ and Na$_2$O in the activator.
[e] Defined as water content in both aqueous activator and water added separately from the activator divided by the sum of precursor and solid activators.

filled into a U-shaped plastic container (approximately 400 mL), and sealed with plastic foil to prevent moisture evaporation. With the ultrasonic signal emitter and receiver installed on two sides of the container, the propagation speed of ultrasonic waves in AAS paste was measured every 30 s to monitor the evolution of structural connectivity along the reaction process. The ultrasonic signal was then processed and recorded by FreshCon system to determine the pulse velocity in the stiffening AAS pastes over time.

2.3.5. Test on fresh properties

As illustrated in Fig. 2, mini-slump and flow curve tests were carried out on AAS pastes every 15 min in the first hour to evaluate the fresh properties. The fresh paste mixtures after mixing were left at rest for further experiments until the target testing age. The time when the first group of tests began was defined as the '0 min', which was 5 min after the wetting of precursors.

Flow curve tests were performed with Anton Paar MCR 102 rheometer (fitted with a 6-blade vane, 22 mm diameter and 16 mm height) to characterize their rheology evolution with time. When the target age of testing was reached, the ready-mixed pastes were filled into the rheometer cup, and the vane was then immersed into fresh paste to conduct the flow curve tests. A plastic lid was applied on the top of rheometer cup to prevent moisture evaporation during each measurement. Flow curve tests were performed at $20 \pm 0.5\,^{\circ}\text{C}$ with a water bath system attached to the rheometer.

As shown in Fig. 3, a high-speed pre-shear was applied at the beginning to break down the structure buildup and recovery between two flow curve tests. Subsequently, the paste remained at rest for 30 s to dissipate the residual stress due to pre-shear [38], followed by the ascending and descending shear rate steps. The response was recorded every second, and the average value of 10 data points was recorded in each step as the corresponding shear stress to derive the flow curves. Dynamic yield stress and plastic viscosity were determined by applying Bingham fitting (Eq. (2)) in the downward portion of each flow curve.

$$\tau = \tau_0 + \mu \cdot \dot{\gamma} \tag{2}$$

where:

τ is the shear stress in Pa.
τ_0 is the dynamic yield stress in Pa.
μ is the plastic viscosity in Pa · s.
$\dot{\gamma}$ is the shear rate in 1/s.

The mini-slump test was performed with a slump cone (38 mm and 60 mm inner dimeter on top and bottom sections, respectively, and 40 mm height) to determine the spread diameter. AAS paste was remixed manually for 30 s before each slump test to ensure a similar shear history as the paste used for flow curve test. For each test, the slump cone was placed on a flat sheet, and fresh AAS paste was poured into the cone until it was completely filled. Afterwards, the cone was lifted as slowly as possible (<1 cm/s) to get rid of inertial effects [39]. The mean value of two diameters in perpendicular directions was recorded as the spread value.

2.3.6. Compressive/flexural strength test

The compressive and flexural strength were tested on mortar level according to EN196-1 to evaluate the strength development of AAS mortars. The w/b ratio of mortar mixtures was fixed at 0.4. CEN-Normsand was applied as the fine aggregate, and the paste to aggre-
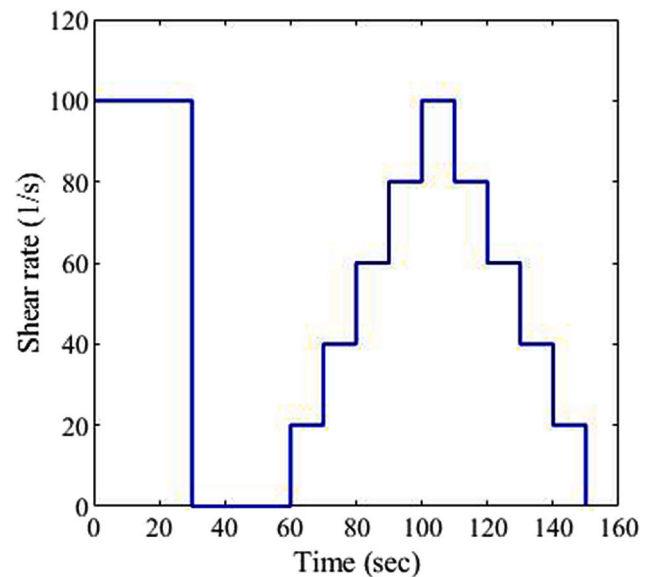

Fig. 3. Shear protocol used in flow curve test.

gate ratio was kept constant at 0.5. The mortar was prepared by premixing dry components (BFS and sand) in a Hobart mixer at low speed (140 rpm) for 2 min. Afterwards, the activator solution was added and the mixture was further mixed at low speed (140 rpm) and high speed (285 rpm) for 60 and 90 s, respectively. Subsequently, the fresh mortar was cast into $40 \times 40 \times 160$ mm molds and vibrated for 15 s to eliminate the entrapped air bubbles. Mortar prisms were demolded after 24 h and sealed with plastic foils, the specimens were placed in a curing chamber at 20 °C with 95% relative humidity. Flexural strength tests were conducted at 1 and 28 days, while the compressive strength was measured at 1, 7, 28, and 91 days, and the average strength of three specimens was reported.

2.3.7. Fourier transform infrared spectroscopy (FTIR)

FTIR spectra were collected with a SHIMADZU IRAffinity-1 spectrometer to analyze the reaction products in AAS pastes. After 1-day sealed curing, the alkali-activation reaction process in AAS pastes was terminated with the wet grinding method described in Refs. [40,41], where the soluble species and water content were extracted from the reaction products, successively. The remaining solid powder was then oven-dried at 50 °C for 24 h. Afterwards, 1 mg AAS samples were further ground together with 100 mg IR-grade KBr and pressed into a thin disc to perform FTIR analysis at a frequency range of 400–4000 cm^{-1}, with a spectral resolution of 1 cm^{-1}.

3. Results and discussion

3.1. Characterization on activator solutions

As presented in Fig. 4, the viscosity of reference tap water was measured as 1.001 mPa s at 20 °C. Among activators with the same modulus, the highest viscosity was detected in S4Ms0.25 and S4Ms0.5 made of SF particles, their viscosity reached 3.891 mPa s and 6.040 mPa s, respectively. This is due to the fact that SF was not completely
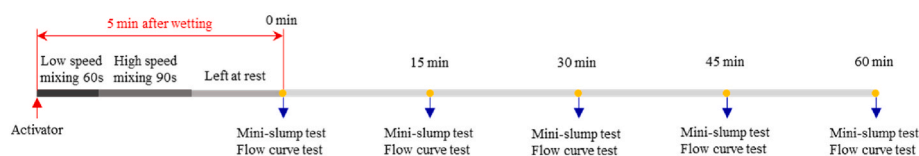

Fig. 2. Testing protocol for fresh properties of AAS pastes.

dissolved (as shown in Fig. 5) so that the collision and friction among remaining solid particles contributed to the interactions as well when external shear was applied. Meanwhile, the activators with the same modulus prepared by SS showed almost identical viscosity, which was about only half of that in SF-based activators. From Ms0.25 to Ms0.5, the viscosity of activators made of SS increased approximately 10%. The higher viscosity referring to high-modulus activators might be attributed to the involvement of more silicate species with a larger molecular size in the activator so that the intermolecular interactions became stronger as well [42].

As shown in Fig. 5, the dissolution of SF particles in alkaline solutions was incomplete after 24 h. Accordingly, the remaining solid SF in S4Ms0.25 and S4Ms0.5 activators were determined and the results are summarized in Table 4. It is evident that the dissolution of SF was limited in both activators, and the dissolution rate of SF in the Ms0.25 activator was higher than that in the Ms0.5 activator. Such difference might be attributed to the high alkalinity in low Ms activators [43], which promoted the dissolution of solid SF.

3.2. Reaction kinetics

3.2.1. Heat evolution

The heat evolution during the exothermic reaction process for each AAS mixture was recorded by calorimeter, and the results of heat flow and cumulative heat release are presented in Fig. 6. Similar to the hydration process of OPC materials, the profile of the curves representing the heat flow of AAS pastes could be divided into five stages, namely: dissolution, induction, acceleration, deceleration, and the steady period [44,45].

In both groups, a rapid reaction process was detected at the early stage in pastes made of SF-based activators. The second exothermic peak referring to acceleration-deceleration periods occurred at around 30 min, which was much earlier than those representing AAS pastes made of SS. In S4Ms0.25, this exothermic peak even merged into the descending phase of the dissolution peak, as indicated by the arrow in Fig. 6(a).

In the case of SS-based mixtures, the AAS pastes exhibited identical heat evolution trends within each group. The results reveal that the activator made of different SS reached the same degree of polysilicate equilibrium, or such process towards an equilibrium (i.e. activator was prepared 24 h before mixing) does not have a major impact on the heat release of the subsequent reaction process. Moreover, the modulus of activator had an obvious impact on the feature of heat evolution along the reaction process. As shown in Fig. 6(a), a short induction period between dissolution and acceleration period was detected in Ms0.25 SS group. The highest heat flow about 1.5 mW/g in the second exothermic peaks occurred at around 5.1 h, while the second exothermic peak lasted
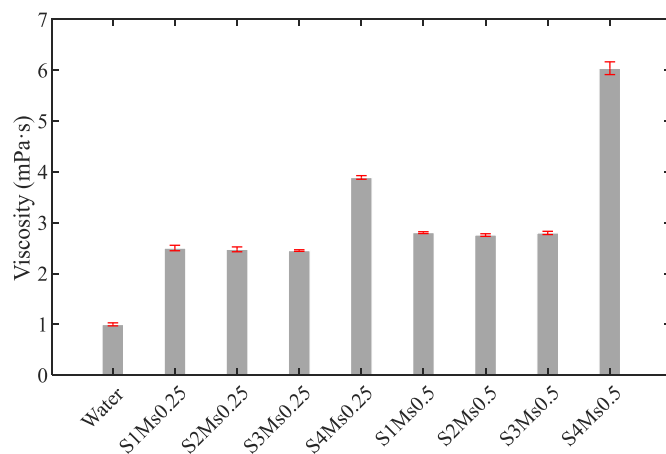

Fig. 5. Activator solutions after 24 h.

Table 4
Properties of SF-based activators after 24 h.

Activator	Initial SF (g)	Undissolved SF (g)	Dissolution rate (%)	Designed Ms	Actual Ms
S4Ms0.25	4	2.44 ± 0.08	39.0	0.25	0.10
S4Ms0.5	8	5.16 ± 0.12	35.5	0.5	0.18

about 11 h. Regarding the heat evolution curves of pastes activated with Ms0.5 SS, a long induction period (approximately 6 h) appeared after dissolution as shown in Fig. 6(a), and the acceleration/deceleration peak was detected from 6 h till the end of measurement (lasted for approximately 18 h). Furthermore, a maximum heat flow value of 1.4 mW/g was detected during the acceleration/deceleration period at around 10 h. Comparing to AAS pastes made of Ms0.25 SS, the induction period of AAS pastes made of high-modulus SS was severely extended. Meantime, the second exothermic peak of heat flow was delayed by 7.5 h, and the maximum heat flow was declined by 6.7%.

S4Ms0.25 and S4Ms0.5 showed more rapid development of cumulative heat release at the very beginning of the reaction process, which is attributed to the rapid exothermic reaction after dissolution. However, the cumulative heat release almost reached the same level at the end of the measurement in each group, while Ms0.5 pastes in general released more heat than Ms0.25 pastes.

The results suggest that AAS pastes with the same nominal composition made from different SS have almost the same exothermic behavior during the reaction process. However, more intensive heat release was observed in pastes with SF-based activators, which might be due to the high alkalinity [29,43] by adding more sodium hydroxide in the activators. Meanwhile, the lower actual Ms (presented in Table 4) also led to more monomers and dimers in the activators, which require less activation energy [46]. On the other hand, by increasing the silicate modulus from 0.25 to 0.5, the exothermic peak was delayed and the maximum heat flow was reduced as well. Moreover, AAS pastes with Ms0.5 activators exhibited more cumulative heat along the reaction process up to 24 h. Therefore, the exothermic reaction became more moderate and stable along the reaction process by providing extra silicate species up to Ms0.5 in the activator.

3.2.2. UPV test

The UPV evolution of AAS measured in this study could be substantially divided into five stages, as indicated in Fig. 7. After the first contact between slag and activators, very steep acceleration and deceleration stages occurred. In all UPV curves, the rapid growth of ultrasonic wave speed was detected in all AAS pastes from the beginning up to 20 min, and speeded up to around 1750 m/s. The observation reveals that a stable and well-connected network was already established in the mixture at an early stage of the reaction process so that the ultrasonic waves could travel at a rather constant high speed in dormant period. Similar UPV evolution has been reported by Cao et al. [41], and they
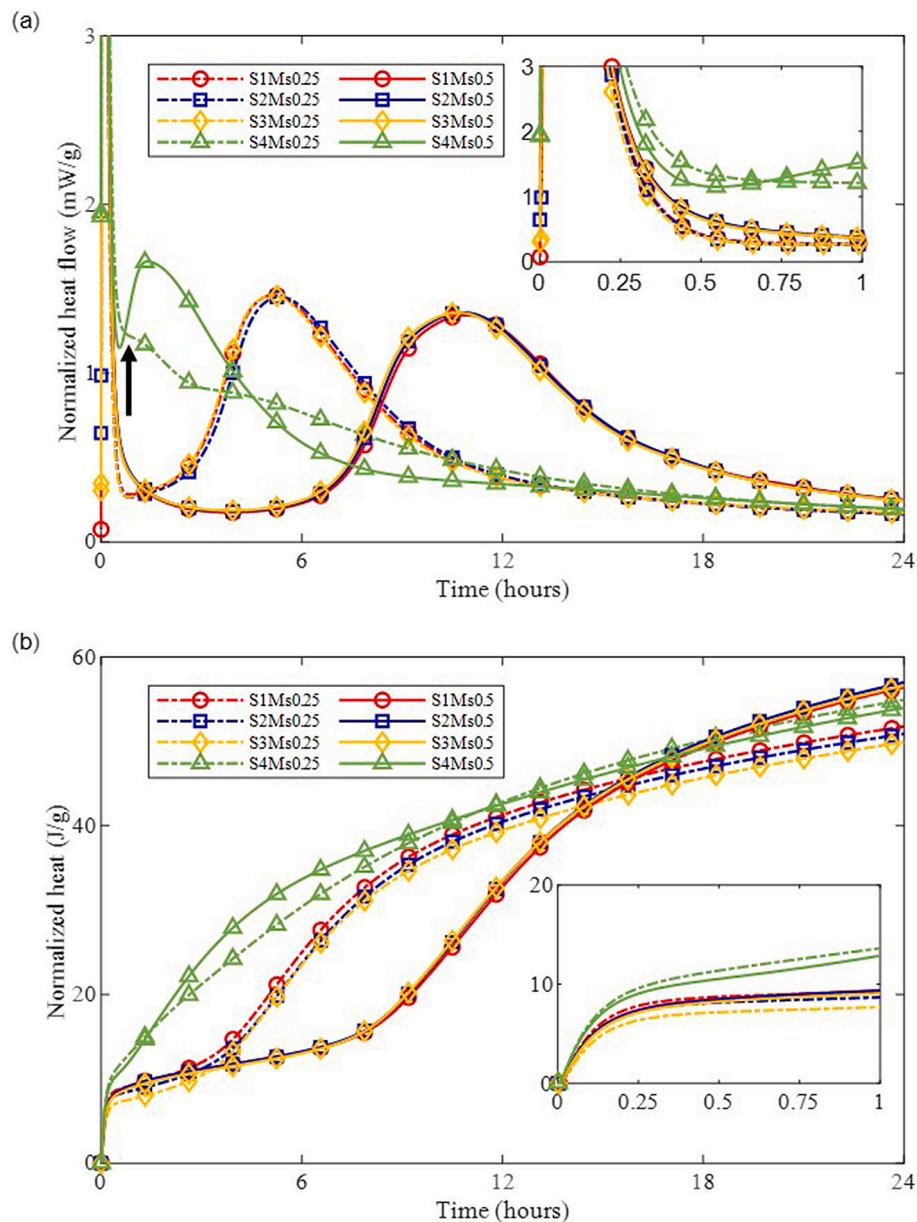

Fig. 4. Viscosity of activator solutions after 24 h.

Fig. 6. Heat evolution of AAS pastes (w/b = 0.4) (a) Normalized heat flow; (b) Cumulative heat.

explained it through their FTIR study that the BFS particles are wrapped by the reaction products generated in the first acceleration period so that the propagation path of ultrasonic waves between solid particles is established. Subsequently, a dormant stage followed, where the UPV reached a plateau, and the structure development in the AAS mixtures was temporarily suspended. On the one hand, the silicate species provided by the activator are gradually consumed by the interaction with calcium content released from slag particles in the previous stage [47]. Moreover, the slag particles are wrapped by the reaction products attached to the surface, and the dissolution of inner unreacted slag particles is inhibited. Accordingly, the interaction between silicate and calcium reached an equilibrium, and the UPV development came to the dormant stage (stage 3 in Fig. 7) [41]. Afterwards, the silicate species dissolved from slag particles are involved in the condensation between calcium and silicates to form C-A-S-H gel products [48], thus the dormant stage was terminated and the secondary acceleration appeared (stage 4 in Fig. 7). Eventually, the chemical reaction reached another equilibrium in the deceleration stage, while the UPV development progressively slowed down and came to a stable level around 2800 m/s (stage 5 in Fig. 7).

UPV rate was taken as the first derivative of time in ultrasonic wave speed. Two characteristic peaks were observed in UPV rate evolution, referring to the first acceleration/deceleration at the very beginning of reaction process and the secondary acceleration/deceleration after dormant stage, respectively.

In both groups, the dormant period in UPV curve almost disappeared in AAS pastes made of SF-based activators. The second peak in UPV rate occurred at around 2.2 and 2.7 h in S4Ms0.25 and S4Ms0.5, respectively, which is much earlier than the equivalent mixtures prepared with SS-based activators. The results indicate that the development of microstructure initiated earlier in SF-based mixtures due to the aforementioned high alkalinity and low actual Ms. Moreover, both the intensity of the second UPV rate peak in SF-based mixtures and their final UPV values are lower than in the corresponding SS-based mixtures. It is likely that the linkages between slag particles are less connective in SF-based mixtures, and the microstructure is less developed and more porous as well.

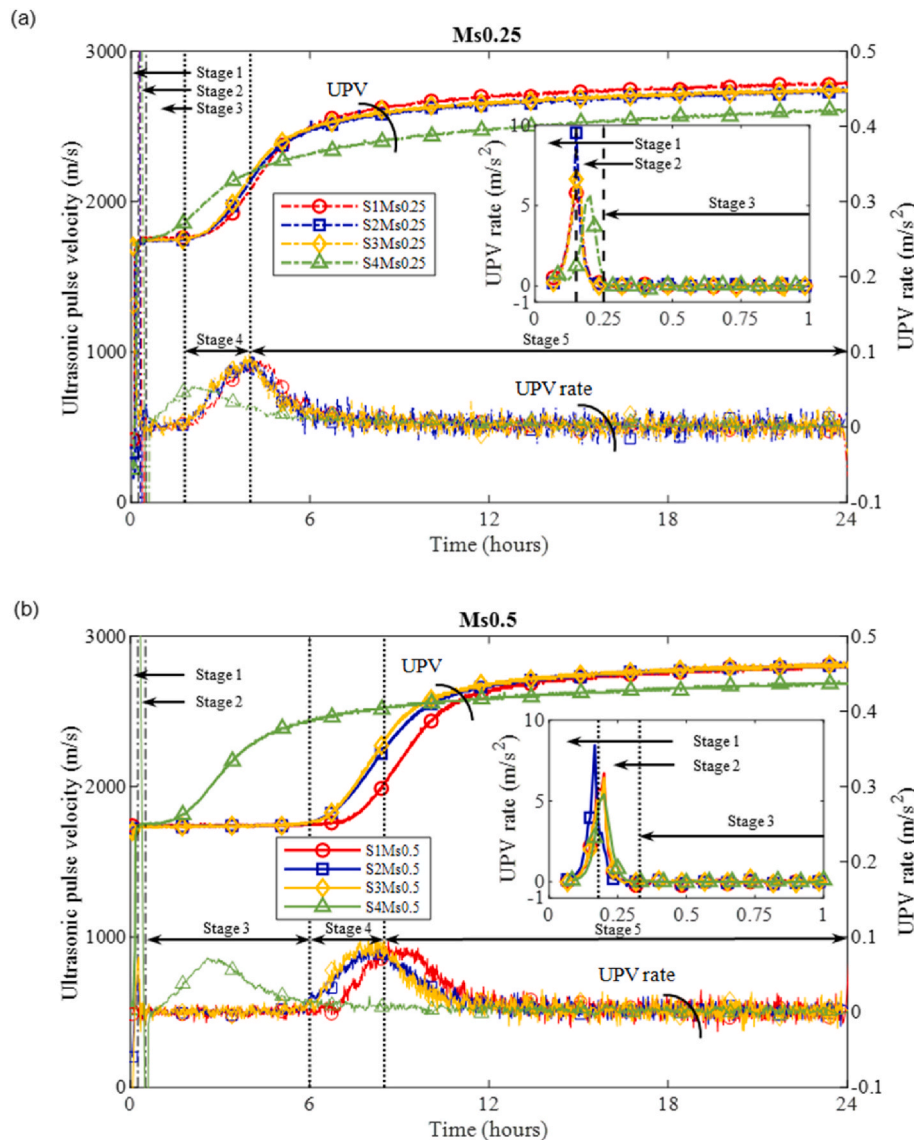As presented in Fig. 7, there is no significant distinction on UPV and

Fig. 7. Ultrasonic pulse velocity and UPV rate against time of AAS pastes (w/b = 0.4) (a) Activator Ms = 0.25; (b) Activator Ms = 0.5.

UPV rate evolution curves in SS-based AAS pastes under the same silicate concentration. In other words, the AAS pastes with the same nominal composition made of different SS showed almost identical features of structural development. Meanwhile, it is noteworthy that the dormant stage was significantly extended by improving the silicate modulus from 0.25 to 0.5. In Ms0.25 SS-based mixtures, the dormant stage started at about 15 min and lasted about 1.5 h till the beginning of the second acceleration, while the dormant stage began at 20 min and ended at about 6 h in Ms0.5 SS-based mixtures.

Regarding both calorimetry and UPV results in each mixture, the time slot where the second UPV rate peak occurred as shown in Fig. 7 nearly coincides with the heat flow peak detected by calorimetry (presented in Fig. 6), while the cumulative heat and UPV evolution almost followed the same trend as well. The results reveal that the microstructure development is associated with the exothermic reaction, and similar observation has been reported by Uppalapati et al. [49] as well. The UPV rate and heat flow are related to the rate of reaction, while UPV and cumulative heat are reflecting the accumulation of reaction products and the maturity of microstructure. However, the microstructural development detected by UPV is slightly earlier than the exothermic reaction recorded by calorimetry, which might be ascribed to the non-exothermic structural development.

3.3. Fresh properties

3.3.1. Mini-slump test

The results of mini-slump tests are presented in Fig. 8. AAS pastes activated by SS exhibited similar trends in spread diameter evolution over time. In SS-activated Ms0.25 pastes, average initial and final spread diameters about 105 and 70 mm were detected at 0 and 60 min, respectively, which declined by 33% after 60 min as the reaction proceeded. Meanwhile, Ms0.5 SS-based mixtures exhibited larger spread diameter (averagely 125 and 105 mm at 0 and 60 min, respectively) and slower slump loss (reduction by 16%) over time. Accordingly, the inclusion of more silicate species in the activator increased the spread value of AAS pastes within the first hour. Moreover, the extra silicate species also slowed down the reaction process, reducing the slope of the slump loss. In AAS mixtures made of SF-based activators, the reaction took place rather fast, and almost no flow was detected in S4Ms0.25 from the very beginning, while the initial spread diameter of S4Ms0.5 was 93 mm and the mixture lost its fluidity after 30 min.

3.3.2. Flow curve tests

Downward portions of flow curves are illustrated in Fig. 9, and each curve is representing the mean value of two measurements. It is evident
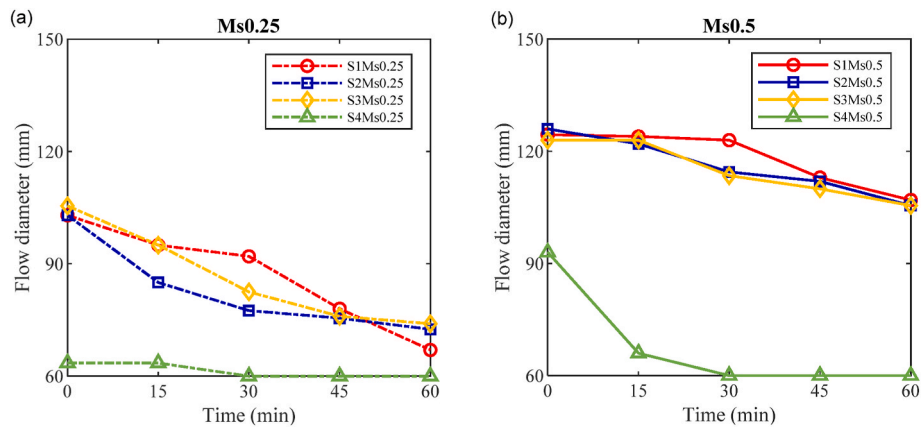
Fig. 8. Flow diameter against time of AAS pastes (a) Activator Ms = 0.25; (b) Activator Ms = 0.5.

that the flow curves in different mixtures descended with time. The results indicate that the structure buildup in AAS mixtures in the first hour was limited and reversible, which was gradually broken down [50] due to the external shear applied.

Dynamic yield stresses of AAS pastes are displayed in Fig. 10. Similar yield stress evolution has been detected among AAS pastes made of SS-based activators, and their yield stress was kept almost constant in the first hour. The mixtures with higher silicate content generally exhibited lower yield stress (approximately 30 Pa) comparing to Ms0.25 mixtures (about 40 Pa). Alonso et al. [51] have also reported a similar fluidizing effect of the sodium silicate. Meanwhile, much larger dynamic yield stress was detected in SF-based mixtures comparing to SS-based mixtures, and their initial yield stress reached about 100 Pa. The results revealed the rapid structural buildup in SF-based mixtures at the very beginning of the reaction process, which might be ascribed to the accumulation of primary C-(A)-S-H gels [50,52,53]. However, the yield stress in S4Ms0.25 and S4Ms0.5 significantly declined to 80 and 65 Pa after 15 min, respectively. It is indicated that in these mixtures, the shear energy induced during the first flow curve test was insufficient to break down the structural development. Afterwards, the reaction entered the induction period and the structure buildup slowed down. In that case, the yield stress dropped down as the interparticle flocs were progressively broken down by the shear forces applied along with the subsequent flow curve tests. Eventually, the yield stress in S4Ms0.25 and S4Ms0.5 slightly increased again as the reaction proceeded, which is associated with the early exothermic process after dissolution detected in calorimetry. However, the reduction in yield stress at around 15 min in SF-based mixtures was not reflected by corresponding mini-slump tests. Probably the manual remixing was not strong enough to break down the structural development, and the spread diameter continuously reduced with time elapsed.

As shown in Fig. 11, lower viscosity was detected in SF-based mixtures comparing to AAS pastes made of SS activators. In the meantime, SS-based mixtures with the same modulus followed very similar trends in plastic viscosity evolution. Ms0.5 mixtures generally exhibited lower plastic viscosity than Ms0.25 mixtures. Furthermore, the plastic viscosity of all AAS mixtures progressively reduced within the first hour, along with the continuous flow curve tests. The primary C-(A)-S-H gel formed progressively, which filled the voids between slag particles and resulted in a better lubrication effect. On the other hand, the reaction reached a dormant period after the rapid dissolution that there was very limited structure development within the first hour. The agglomerations were progressively broken down into smaller particles due to the shear applied. Therefore, a gradual decline in plastic viscosity was detected among all AAS pastes. Besides, it is noteworthy that the silicate content resulted in opposite effects on the viscosity of activator solutions and AAS pastes. Higher viscosity was detected in the activator with increasing Si modulus [54], while AAS pastes prepared with high Ms

activators showed lower viscosity. It is indicated that the extra silicate species remained as liquid gels at the early stage, which reduced the solid concentration in fresh AAS mixtures and led to lower viscosity [55].

Among all AAS pastes, SF-based mixtures showed higher dynamic yield stress but lower viscosity than SS-based mixtures in the first hour. In SF-based mixtures, the high yield stress is attributed to the aforementioned rapid dissolution enabling a fast microstructure development within the first hour. Besides, the undissolved SF particles further increased the solid fraction, which resulted in more flocculation as the reaction proceeded [56]. Hence, a stronger external shear is required to break down the interparticle linkages and initiate the flow [57]. Nevertheless, lower plastic viscosity was detected in SF-based mixtures, which is due to the undissolved silica fume in the activators. These solid spherical silica particles would provide a ball-bearing effect [58] and disperse the slag particles. However, in the case of SS-based mixtures, the liquid activator would be easily deformed and squeezed out from interparticle phases when undergoes external shear forces. Therefore, SF particles would better mitigate the contact between slag particles, and thus lower viscosity was detected in SF-based mixtures.

To sum up, AAS paste with the same nominal composition made of SS-based activators showed very similar fresh properties along the reaction process in terms of mini-slump spread, dynamic yield stress and plastic viscosity. However, some distinctions in results have been observed among different mixtures, as the result might be sensitive to the energy induced during remixing and refilling of fresh pastes [59]. Meanwhile, the reaction was slowed down and rheological parameters were improved by increasing silicate modulus from 0.25 to 0.5. The silicate species from the activators and primary C-(A)-S-H gel formed at the beginning of reaction were wrapped around the slag particles [41], which behaved as a lubricating phase to disperse the slag particles [52, 60]. Subsequently, these primary gel structures further polymerized and condensed into solid reaction products. Macroscopically, the setting of the AAS paste occurred and the fresh mixture gradually lost its fluidity. In the case of SF-based mixtures, fresh properties deteriorated rapidly since dissolution took place very fast in high-alkalinity activators, and the reactants soon reached their supersaturation to condense into solid reaction products. Furthermore, the undissolved solid SF also provided ball bearing effects to reduce the viscosity of AAS mixtures.

3.4. Hardened properties

3.4.1. Compressive and flexural strength development

The compressive strength of AAS mortar specimens is presented in Fig. 12(a). In AAS with Ms0.25 group, the compressive strength was approximately identical among all samples activated by SS. Their 1-day and 91-day compressive strength reached about 18 MPa and 58 MPa, respectively. Meanwhile, the reduction in strength development was
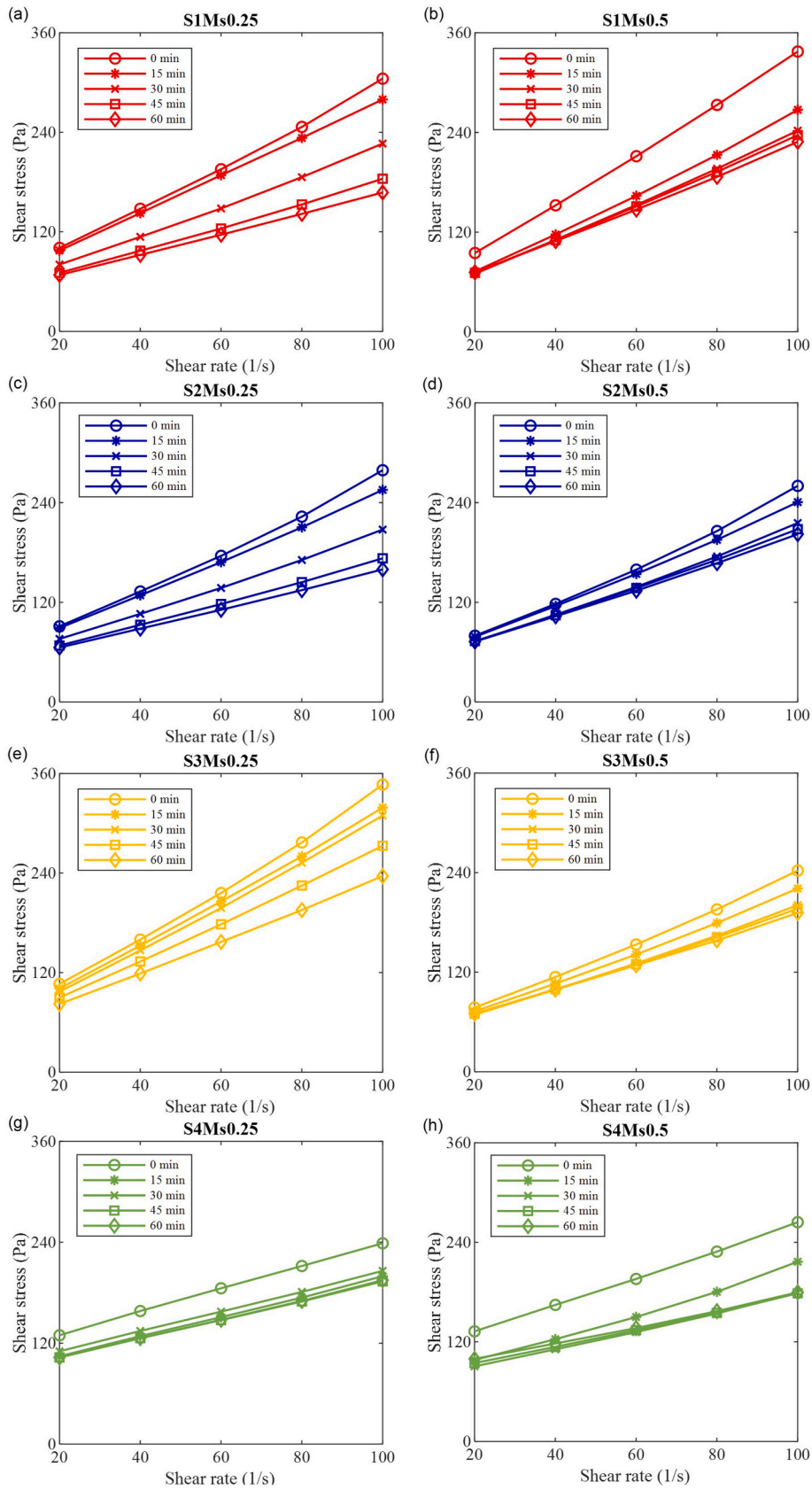
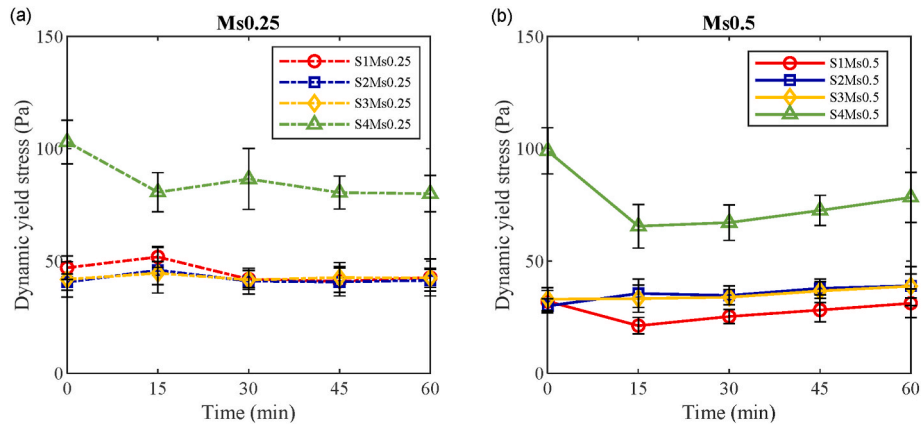**Fig. 9.** Flow curves of AAS pastes (shear stress - shear rate).

Fig. 10. Dynamic yield stress against time of AAS pastes (w/b = 0.4) (a) Activator Ms = 0.25; (b) Activator Ms = 0.5.
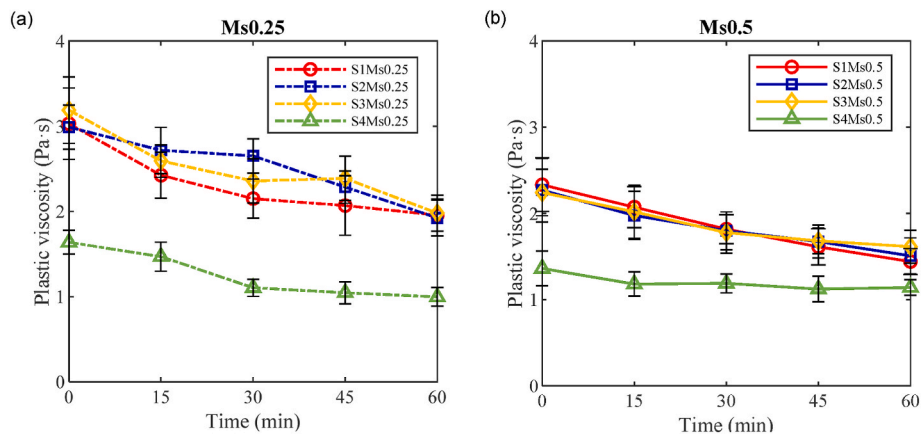

Fig. 11. Plastic viscosity against time of AAS pastes (w/b = 0.4) (a) Activator Ms = 0.25; (b) Activator Ms = 0.5.

observed when using SF to prepare the activator. This might be attributed to that the dissolution of SF was incomplete, and the actual Ms in SF-based activators was lower than SS-based activators. Therefore, the compressive strength declined by 39% and 28% at 1 and 91 days, respectively. Meanwhile, the strength development was further enhanced by improving the silicate concentration in the activator up to Ms0.5 at all curing ages. An average ultimate strength among S1Ms0.5, S2Ms0.5, and S3Ms0.5 about 81.5 MPa was detected at 91 days, which was improved by 41% comparing to Ms0.25 specimens. Furthermore, the addition of extra silicate especially resulted in more strength development in the late curing stage from 7 to 91 days, comparing to

Ms0.25 mixtures. In S4Ms0.5, the strength was once again reduced by using SF-based activators.

As illustrated in Fig. 12(b), a similar development trend was obtained in flexural strength. SS resulted in higher strength than SF-based activators. In Ms0.25 group, the average flexural strength reached 4.34 MPa and 5.62 MPa in specimens activated by SS, while 3.54 MPa and 4.14 MPa were detected in specimens made of SF-based activators at 1 and 28 days, respectively. Moreover, there were no obvious distinctions on 1-day flexural strength (averagely 4.84 MPa) between solid and liquid sodium silicate sources in Ms0.5 group. However, an average of 9.36 MPa 28-day flexural strength was detected among samples activated by
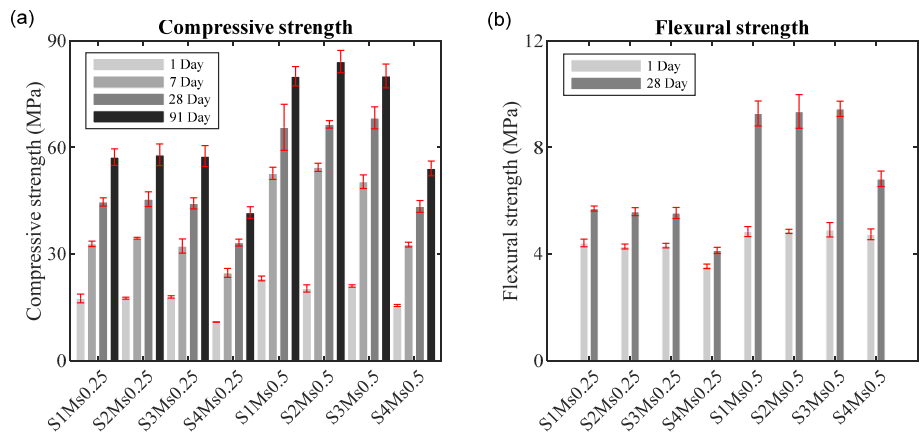

Fig. 12. Strength development of AAS mortars (a) Compressive strength; (b) Flexural strength.

SS, while S4Ms0.5 only reached 6.83 MPa. It is evident that aqueous SS enhanced flexural strength development from 1 to 28 days, while the impact on first-day strength development was limited. In the case of SS as the activator, the 1-day flexural strength increased by 12% by doubling the silicate modulus in the activator, and the 28-day flexural strength improved by 67%.

Regarding both compressive and flexural strength development, the specimens made of SS exhibited higher strength at all corresponding ages than those made of SF. The results indicate that aqueous silicate source is more reactive and effective than that in a solid form, and there is no significant impact on the strength development by using different SS to prepare the activator. On the other hand, higher modulus activators did not result in much improvement in 1-day strength but further enhanced the strength development in later stages with higher ultimate strength. According to the SEM observations [22], the extra silicate content originating from the activator will continuously provide nucleation sites [44] for the reaction products, and contribute to higher strength pastes with a denser and more homogenous microstructure.

3.4.2. FTIR analysis

FTIR analysis was performed to check the reaction products since the majority of them are amorphous phases [61,62]. Results of FTIR spectra on 1-day AAS pastes are shown in Fig. 13. Compared to the spectrum representing BFS, a rather wide band at 3450 cm^{-1} together with a sharp absorption peak at around 1650 cm^{-1} were detected in all AAS samples. They are associated with the stretching and bending vibration of O–H [63,64], respectively, which is attributed to the chemically bound water during the alkali-activation process [65]. Besides, distinctive peaks at around 1488 cm^{-1} and 1425 cm^{-1} were detected in AAS samples after the activation process. Those absorption peaks are associated with the vibration of O–C–O bonds [41], which were scarcely detected in BFS. Such observation indicates that C–S–H underwent decalcification to form calcium carbonates [66]. Furthermore, typical characteristics of Si–O bands were detected at around 501 cm^{-1} and 949 cm^{-1}, assigned to the bending vibration of Si–O in silicon-oxygen tetrahedrons and stretching vibration of Si–O bond [48], respectively. The feature of these bands is regarded as an indicator of the activation process [61]. Upon alkali-activation, both of them became less intensive. The absorption band originally located at 949 cm^{-1} in BFS shifted towards higher wavenumbers while the other band at 501 cm^{-1} moved into a lower wavenumber region. In addition, the characteristic peak that occurred at around 700 cm^{-1} ascribed to the vibration of Al–O bonds, resulted from the substitution of silicon by aluminum within silicon-oxygen tetrahedron structures [48].

In either low or high silicate modulus groups, it has been observed that AAS samples made of SS exhibited very similar spectral features. Their characteristic peaks referring to Si–O vibration at 501 cm^{-1} and

949 cm^{-1} shifted towards the corresponding directions to a greater extent than SF-based samples. It can be linked to the strength development SS-based samples showing higher strength than SF-based samples with the same nominal composition after 1-day curing. Regarding the effect of different silicate modulus in SS-based samples, the Si–O bending vibration band at 501 cm^{-1} moved to around 460 cm^{-1} and 440 cm^{-1} in Ms0.25 and Ms0.5 samples, respectively. While the Si–O stretching peak at 949 cm^{-1} shifted towards about 955 cm^{-1} and 960 cm^{-1} in Ms0.25 and Ms0.5 samples, respectively. Accordingly, higher silicate content in the activator also resulted in more peak shifts in Si–O characteristic vibrations. This observation is in agreement with other studies [41,61]. The results also reveal that more reactive silicate content in the activators would contribute to a higher degree of alkali-activation, leading to more reaction products and higher strength. However, this contribution is rather limited to the range Ms0.25 to Ms0.5 investigated in this study. Excessive silicate species might on the other hand lead to insufficient alkalinity of the activator [67], and subsequently inhibit the dissolution of precursors as well as the alkali-activation process.

4. Conclusions

In this research, a comprehensive study has been carried out to check the reproducibility of alkali-activated slag (AAS) mixtures, and the activators were made of different silicate sources with the same nominal composition. The following conclusions could be made according to the results of reaction kinetics, rheology and strength development:

- AAS pastes made from different commercial sodium silicate solutions (SS) within this study exhibited no obvious distinction on reaction kinetics, fresh properties and strength development features with time.
- The activator made through the preparation protocol described in this study provided equivalent performance in AAS pastes, and the reproducibility of AAS with different SS sources has been proved.
- Silicate species in the aqueous SS could provide a lubricating effect in AAS paste, and activators with high silicate content in this study reduced both dynamic yield stress and plastic viscosity (approximately reduced by 25% and 23% at 0 min, respectively) of AAS paste within the first hour.
- Certain impact on the reaction kinetics has been observed by improving silicate modulus from 0.25 to 0.5, the dormant/induction period was obviously extended.
- High silicate content in the activator resulted in more strength development from 7 to 91 days in hardened AAS mortars. In SS-based AAS, the ultimate compressive strength in Ms0.25 and Ms0.5 mixtures reached about 60 MPa and 80 MPa after 91 days, respectively.
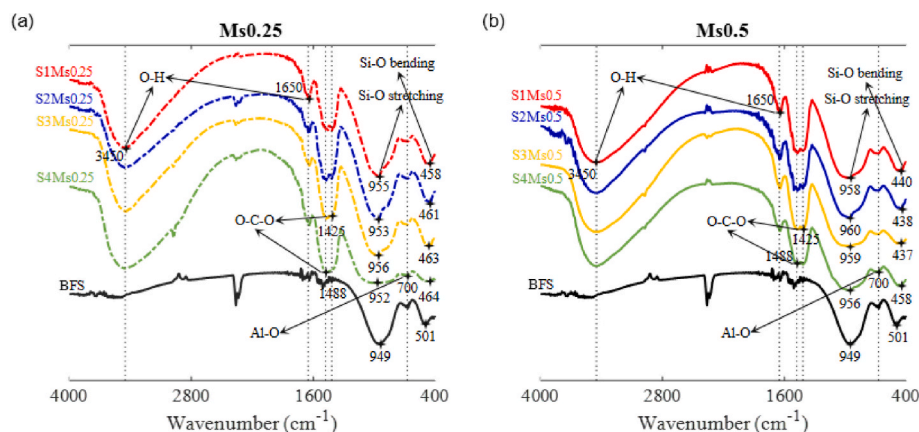

Fig. 13. FTIR spectra of AAS pastes (a) Activator Ms = 0.25; (b) Activator Ms = 0.5.

- AAS mixtures prepared with silica fume (SF) activators showed higher yield stress and more rapid slump loss than corresponding SS-based mixtures, due to the high alkalinity and fast reaction process in the early stage. However, SF-based mixtures developed less compressive strength at the same curing ages compared to SS-based mixtures, since the dissolution of silicate source was incomplete.
- The undissolved SF particles provided a ball-bearing effect, which resulted in a reduction in plastic viscosity compared to SS-based mixtures. It is feasible to use SF as a mineral admixture to improve the rheological properties of AAS mixtures.

CRediT authorship contribution statement

Yubo Sun: Conceptualization, Methodology, Investigation, Writing - original draft. **Saeid Ghorbani:** Investigation, Writing - original draft. **Xiaodi Dai:** Conceptualization, Methodology, Writing - original draft. **Guang Ye:** Supervision, Writing – review & editing. **Geert De Schutter:** Funding acquisition, Supervision, Writing – review & editing.

Declaration of competing interest

The authors declare that they have no known competing financial interests or personal relationships that could have appeared to influence the work reported in this paper.

Acknowledgments

References

[1] J.L. Provis, J.S.J. Van Deventer, Alkali Activated Materials: State-Of-The-Art Report, RILEM TC 224-AAM, Springer Science & Business Media, 2013.

[2] T. Luukkonen, Z. Abdollahnejad, J. Yliniemi, P. Kinnunen, M. Illikainen, Cement and Concrete Research One-Part Alkali-Activated Materials : A review, 103, 2018, pp. 21–34, https://doi.org/10.1016/j.cemconres.2017.10.001.

[3] J.L. Provis, Alkali-activated materials, Cement Concr. Res. 114 (2018) 40–48, https://doi.org/10.1016/j.cemconres.2017.02.009.

[4] C. Shi, A.F. Jiménez, A. Palomo, Cement and Concrete Research New cements for the 21st century : the pursuit of an alternative to Portland cement, Cement Concr. Res. 41 (2011) 750–763, https://doi.org/10.1016/j.cemconres.2011.03.016.

[5] P. Duxson, J.L. Provis, G.C. Lukey, J.S.J. Van Deventer, The role of inorganic polymer technology in the development of ' green concrete, 37, 2007, pp. 1590–1597, https://doi.org/10.1016/j.cemconres.2007.08.018.

[6] P. Duxson, D.G. Brice, Chemical research and climate change as drivers in the commercial adoption of alkali activated materials, 2010, pp. 145–155, https://doi.org/10.1007/s12649-010-9015-9.

[7] A. Fernández-Jiménez, J.G. Palomo, F. Puertas, Alkali-activated slag mortars: mechanical strength behaviour, Cement Concr. Res. 29 (1999) 1313–1321, https://doi.org/10.1016/S0008-8846(99)00154-4.

[8] T.A. Aiken, W. Sha, J. Kwasny, M.N. Soutsos, Cement and Concrete Research Resistance of geopolymer and Portland cement based systems to silage ef fluent attack, Cement Concr. Res. 92 (2017) 56–65, https://doi.org/10.1016/j.cemconres.2016.11.015.

[9] M. Albitar, M.S.M. Ali, P. Visintin, M. Drechsler, Durability evaluation of geopolymer and conventional concretes, Construct. Build. Mater. 136 (2017) 374–385, https://doi.org/10.1016/j.conbuildmat.2017.01.056.

[10] K. Sagoe-Crentsil, T. Brown, A. Taylor, Drying shrinkage and creep performance of geopolymer concrete, J. Sustain. Cem. Mater. 2 (2013) 35–42.

[11] J.L. Provis, A. Palomo, C. Shi, Cement and concrete research advances in understanding alkali-activated materials, Cement Concr. Res. 78 (2015) 110–125, https://doi.org/10.1016/j.cemconres.2015.04.013.

[12] A. Mehta, R. Siddique, An overview of geopolymers derived from industrial by-products, Construct. Build. Mater. 127 (2016) 183–198, https://doi.org/10.1016/j.conbuildmat.2016.09.136.

[13] R.D. Hooton, Cement and Concrete Research Current developments and future needs in standards for cementitious materials, Cement Concr. Res. 78 (2015) 165–177, https://doi.org/10.1016/j.cemconres.2015.05.022.

[14] P. Duxson, A. Fernández-Jiménez, J.L. Provis, G.C. Lukey, A. Palomo, J.S.J. Van Deventer, Geopolymer technology: the current state of the art, J. Mater. Sci. 42 (2007) 2917–2933, https://doi.org/10.1007/s10853-006-0637-z.

[15] Activating solution chemistry for geopolymers, (n.d.) 50–71. https://doi.org/10.1533/9781845696382.1.50.

[16] S. Liu, W.K. Ott, Sodium silicate applications in oil, gas & geothermal well operations, J. Petrol. Sci. Eng. 195 (2020) 107693, https://doi.org/10.1016/j.petrol.2020.107693.

[17] X. Yang, W. Zhu, Q. Yang, The viscosity properties of sodium silicate solutions, J. Solut. Chem. 37 (2008) 73–83, https://doi.org/10.1007/s10953-007-9214-6.

[18] J. Nordström, E. Nilsson, P. Jarvol, M. Nayeri, A. Palmqvist, J. Bergenholtz, A. Matic, Journal of Colloid and Interface Science Concentration- and pH-dependence of highly alkaline sodium silicate solutions 356 (2011) 37–45, https://doi.org/10.1016/j.jcis.2010.12.085.

[19] D. Böschel, M. Janich, H. Roggendorf, Size distribution of colloidal silica in sodium silicate solutions investigated by dynamic light scattering and viscosity measurements, J. Colloid Interface Sci. 267 (2003) 360–368, https://doi.org/10.1016/j.jcis.2003.07.016.

[20] D. Dimas, I. Giannopoulou, D. Panias, Polymerization in sodium silicate solutions: a fundamental process in geopolymerization technology, J. Mater. Sci. 44 (2009) 3719–3730, https://doi.org/10.1007/s10853-009-3497-5.

[21] I.L. Svensson, S. Sjöberg, L.-O. Öhman, Polysilicate equilibria in concentrated sodium silicate solutions, J. Chem. Soc. Faraday Trans. 1 Phys. Chem. Condens. Phases. 82 (1986) 3635–3646.

[22] P. Duxson, J.L. Provis, G.C. Lukey, S.W. Mallicoat, W.M. Kriven, J.S.J. Van Deventer, Understanding the relationship between geopolymer composition, microstructure and mechanical properties, Colloids Surfaces A Physicochem. Eng. Asp. 269 (2005) 47–58, https://doi.org/10.1016/j.colsurfa.2005.06.060.

[23] G. Engelhardt, D. Zeigan, H. Jancke, D. Hoebbel, Sup 29 Si-NMR spectroscopy of silicate solutions: II, Dependence of the structure of silicate anions in water solutions on the Na: Si ratio, Zeitschrift Fur Anorg. Und Allg. Chemie. 418 (1975) 17–28.

[24] M.A. McGarry, J.F. Hazel, Electron microscopy of labile alkali silicate solutions, J. Colloid Sci. 20 (1965) 72–80.

[25] J.L. Bass, G.L. Turner, 29 SI Anion Distributions in Sodium Silicate Solutions . Characterization by Infrared Spectroscopies , and Vapor Phase Osmometry, 5647, 1997, pp. 10638–10644.

[26] M. Dietzel, E. Usdowski, Depolymerization of soluble silicate in dilute aqueous solutions, Colloid Polym. Sci. 273 (1995) 590–597.

[27] K.R. Iler, The Chemistry of Silica: Solubility, Polymerization, Colloid and Surface Properties, and Biochemistry., book published by Wiley & Sons, New York, 1979. ISBN: 978-0-471-02404-0.

[28] C. Shi, D. Roy, P. Krivenko, Alkali-activated Cements and Concretes, CRC press, 2003.

[29] K. Sagoe-Crentsil, L. Weng, Dissolution processes, hydrolysis and condensation reactions during geopolymer synthesis: Part II. High Si/Al ratio systems, J. Mater. Sci. 42 (2007) 3007–3014, https://doi.org/10.1007/s10853-006-0818-9.

[30] X. Dai, S. Aydın, M. Yücel, K. Lesage, G. De Schutter, Cement and Concrete Research Effects of activator properties and GGBFS/FA ratio on the structural build-up and rheology of AAC, Cement Concr. Res. 138 (2020), 106253, https://doi.org/10.1016/j.cemconres.2020.106253.

[31] H. Jansson, D. Bernin, K. Ramser, Silicate Species of Water Glass and Insights for Alkali-Activated Green Cement, 2017, 067167, https://doi.org/10.1063/1.4923371.

[32] S. Aydın, B. Baradan, Effect of activator type and content on properties of alkali-activated slag mortars, Compos. B Eng. 57 (2014) 166–172.

[33] A.M. Humad, A. Kothari, J.L. Provis, A. Cwirzen, The effect of blast furnace slag/fly ash ratio on setting, strength, and shrinkage of alkali-activated pastes and concretes, Front. Mater. 6 (2019) 9.

[34] M. Criado, A. Fernández-Jiménez, A. Palomo, I. Sobrados, J. Sanz, Effect of the SiO2/Na2O ratio on the alkali activation of fly ash. Part II: 29Si MAS-NMR Survey, Microporous Mesoporous Mater. 109 (2008) 525–534, https://doi.org/10.1016/j.micromeso.2007.05.062.

[35] S. Zhang, Z. Li, B. Ghiassi, S. Yin, G. Ye, Fracture properties and microstructure formation of hardened alkali-activated slag/fly ash pastes, Cement Concr. Res. 144 (2021), 106447.

[36] X. Dai, S. Aydın, M.Y. Yardımcı, K. Lesage, G. De Schutter, Rheology and microstructure of alkali-activated slag cements produced with silica fume activator, Cement Concr. Compos. (2021), 104303.

[37] H.W. Reinhardt, C.U. Grosse, Continuous monitoring of setting and hardening of mortar and concrete, Construct. Build. Mater. 18 (2004) 145–154, https://doi.org/10.1016/j.conbuildmat.2003.10.002.

[38] A. Kashani, J.L. Provis, G.G. Qiao, J.S.J. Van Deventer, The interrelationship between surface chemistry and rheology in alkali activated slag paste, Construct. Build. Mater. 65 (2014) 583–591, https://doi.org/10.1016/j.conbuildmat.2014.04.127.

[39] J. Gao, A. Fourie, Spread is better : an investigation of the mini-slump test, Miner. Eng. 71 (2015) 120–132, https://doi.org/10.1016/j.mineng.2014.11.001.

[40] X. Chen, A. Meawad, L.J. Struble, Method to Stop Geopolymer Reaction 3275 (2014) 3270–3275, https://doi.org/10.1111/jace.13071.

[41] R. Cao, S. Zhang, N. Banthia, Y. Zhang, Z. Zhang, Interpreting the early-age reaction process of alkali-activated slag by using combined embedded ultrasonic measurement, thermal analysis, XRD, FTIR and SEM, Compos. B Eng. 186 (2020) 107840, https://doi.org/10.1016/j.compositesb.2020.107840.

[42] B. Averill, P. Eldredge, General Chemistry: Principles, Patterns, and Applications, 2011.

[43] J.-J. Chang, A study on the setting characteristics of sodium silicate-activated slag pastes, Cement Concr. Res. 33 (2003) 1005–1011.

[44] B.S. Gebregziabiher, R. Thomas, S. Peethamparan, Very early-age reaction kinetics and microstructural development in alkali-activated slag, Cement Concr. Compos. 55 (2015) 91–102, https://doi.org/10.1016/j.cemconcomp.2014.09.001.

[45] K.L. Scrivener, A. Nonat, Cement and Concrete Research Hydration of cementitious materials , present and future, Cement Concr. Res. 41 (2011) 651–665, https://doi.org/10.1016/j.cemconres.2011.03.026.

[46] J. Aupoil, J.-B. Champenois, J.-B. d'Espinose de Lacaillerie, A. Poulesquen, Interplay between silicate and hydroxide ions during geopolymerization, Cement Concr. Res. 115 (2019) 426–432.

[47] Y. Zuo, G. Ye, Preliminary interpretation of the induction period in hydration of sodium hydroxide/silicate activated slag, Materials 13 (2020) 1–19, https://doi.org/10.3390/ma13214796.

[48] F. Puertas, A. Fernández-Jiménez, M.T. Blanco-Varela, Pore solution in alkali-activated slag cement pastes. Relation to the composition and structure of calcium silicate hydrate, Cement Concr. Res. 34 (2004) 139–148, https://doi.org/10.1016/S0008-8846(03)00254-0.

[49] S. Uppalapati, L. Vandewalle, Ö. Cizer, Monitoring the setting process of alkali-activated slag-fly ash cements with ultrasonic P-wave velocity, Construct. Build. Mater. 271 (2021) 121592, https://doi.org/10.1016/j.conbuildmat.2020.121592.

[50] M. Palacios, P.F.G. Banfill, F. Puertas, Rheology and setting of alkali-activated slag pastes and mortars: effect if organic admixture, ACI Mater. J. 105 (2008) 140–148, https://doi.org/10.14359/19754.

[51] M.M. Alonso, S. Gismera, M.T. Blanco, M. Lanzón, F. Puertas, Alkali-activated mortars: workability and rheological behaviour, Construct. Build. Mater. 145 (2017) 576–587, https://doi.org/10.1016/j.conbuildmat.2017.04.020.

[52] M. Palacios, S. Gismera, M.M. Alonso, J.B. Espinose, D. Lacaillerie, B. Lothenbach, A. Favier, C. Brumaud, F. Puertas, Cement and Concrete Research Early reactivity of sodium silicate-activated slag pastes and its impact on rheological properties, Cement Concr. Res. 140 (2021), 106302, https://doi.org/10.1016/j.cemconres.2020.106302.

[53] F. Puertas, C. Varga, M.M. Alonso, Rheology of alkali-activated slag pastes. Effect of the nature and concentration of the activating solution, Cement Concr. Compos. 53 (2014) 279–288, https://doi.org/10.1016/j.cemconcomp.2014.07.012.

[54] M.F. Alnahhal, T. Kim, A. Hajimohammadi, Distinctive rheological and temporal viscoelastic behaviour of alkali-activated fly ash/slag pastes: a comparative study with cement paste, Cement Concr. Res. 144 (2021), 106441, https://doi.org/10.1016/j.cemconres.2021.106441.

[55] L. Struble, G.-K. Sun, Viscosity of Portland cement paste as a function of concentration, Adv. Cement Base Mater. 2 (1995) 62–69.

[56] N. Roussel, A. Lemaître, R.J. Flatt, P. Coussot, Steady state flow of cement suspensions: a micromechanical state of the art, Cement Concr. Res. 40 (2010) 77–84, https://doi.org/10.1016/j.cemconres.2009.08.026.

[57] G.H. Tattersall, P.F.G. Banfill, The Rheology of Fresh Concrete, 1983.

[58] H. Vikan, H. Justnes, Rheology of cementitious paste with silica fume or limestone, Cement Concr. Res. 37 (2007) 1512–1517, https://doi.org/10.1016/j.cemconres.2007.08.012.

[59] L. Struble, Rheological changes associated with setting of cement paste, Adv. Cement Base Mater. 2 (1995) 224–230, https://doi.org/10.1016/1065-7355(95)00017-l.

[60] Y. Tian, C. Yang, S. Yuan, H. Yuan, K. Yang, L. Yu, M. Zhang, X. Zhu, Understanding the rheological properties of alkali-activated slag pastes from the cohesion and friction interactions, Construct. Build. Mater. 291 (2021), 123311.

[61] L.Y. Yang, Z.J. Jia, Y.M. Zhang, J.G. Dai, Effects of nano-TiO2 on strength, shrinkage and microstructure of alkali activated slag pastes, Cement Concr. Compos. 57 (2015) 1–7, https://doi.org/10.1016/j.cemconcomp.2014.11.009.

[62] I. Lecomte, C. Henrist, M. Li, F. Maseri, A. Rulmont, R. Cloots, (Micro) -structural comparison between geopolymers , alkali-activated slag cement and Portland cement, 26, 2006, pp. 3789–3797, https://doi.org/10.1016/j.jeurceramsoc.2005.12.021.

[63] N. Li, N. Farzadnia, C. Shi, Microstructural changes in alkali-activated slag mortars induced by accelerated carbonation, Cem. Concr. Res. 100 (2017) 214–226, https://doi.org/10.1016/j.cemconres.2017.07.008.

[64] K. Il Song, J.K. Song, B.Y. Lee, K.H. Yang, Carbonation characteristics of alkali-activated blast-furnace slag mortar, Adv. Mater. Sci. Eng. 2014 (2014), https://doi.org/10.1155/2014/326458.

[65] S.A. Bernal, R.M. de Gutierrez, J.L. Provis, V. Rose, Effect of silicate modulus and metakaolin incorporation on the carbonation of alkali silicate-activated slags, Cement Concr. Res. 40 (2010) 898–907, https://doi.org/10.1016/j.cemconres.2010.02.003.

[66] F. Puertas, M. Palacios, T. Vázquez, Carbonation process of alkali-activated slag mortars, J. Mater. Sci. 41 (2006) 3071–3082, https://doi.org/10.1007/s10853-005-1821-2.

[67] D. Krizan, B. Zivanovic, Effects of dosage and modulus of water glass on early hydration of alkali, – slag cements 32 (2002) 1181–1188.